

# Electron Cloud Density Measurements in Accelerator Beam-pipe Using Resonant Microwave Excitation

J.P. Sikora<sup>a,\*</sup>, S. De Santis<sup>b</sup>

<sup>a</sup>CLASSE, Cornell University, Ithaca, New York 14853 United States

<sup>b</sup>LBNL, Berkeley, California 94720, United States

## Abstract

An accelerator beam can generate low energy electrons in the beam-pipe, generally called electron cloud, that can produce instabilities in a positively charged beam. One method of measuring the electron cloud density is by coupling microwaves into and out of the beam-pipe and observing the response of the microwaves to the presence of the electron cloud. This paper describes a technique in which the beam-pipe is resonantly excited with microwaves and the electron cloud density calculated from the change that it produces in the resonant frequency of the beam-pipe. The resonant technique has the advantage that measurements can be localized to sections of beam-pipe that are a meter or less in length, as well as greatly improving the signal to noise ratio.

**Keywords:** accelerator, storage ring, electron cloud, plasma, microwave, resonance

## 1. Introduction

An accelerator beam can generate low energy electrons by ionization of the residual gas in the beam-pipe or from the photo-electrons produced by synchrotron radiation. These electrons can then produce secondary electrons, generating an electron cloud (EC) that can result in instabilities and emittance growth in a positively charged accelerator beam [1, 2]. Several techniques have been developed to measure the EC density in order to test mitigation techniques and for comparison with the results of numerical simulations [3, 4].

One of these techniques couples microwaves into the beam-pipe and uses the interaction of electrons with the microwaves to measure the EC density. When this technique was first introduced, the microwaves were propagated for some distance through the beam-pipe before being observed with a spectrum analyzer. The result is a change in the phase shift per unit length that is proportional to the EC density [5–8]. For a periodic EC density, such as that produced by a short train of bunches in a storage ring, this results in phase modulation of the received signal. These measurements generally use the fundamental mode propagating in the beam-pipe and therefore are commonly referred to as the TE wave technique of electron cloud measurement.

In practice, transitions in the cross-section of the beam-pipe for accelerator hardware such as wigglers and gate valves produce reflections of the wave. Longitudinal slots used to connect vacuum pumps to the beam-pipe vacuum also produce reflections. So single pass transmission of TE waves from point to point through the beam-pipe is not commonly achieved at fre-

quencies near the beam-pipe cutoff, making the length of propagation difficult to determine.

Figure 1 shows an example from the Cornell Electron Storage Ring Test Accelerator (CESRTA) [9], where reflections are generated by the longitudinal slots at vacuum pumps. For this measurement, the microwaves are coupled in and out of the beam-pipe at the same longitudinal position using buttons normally connected to the beam position monitor (BPM) system. The resonant response is the result of reflections from the longitudinal slots. Resonances occur at the frequencies  $f^2 = f_c^2 + (nc/2L)^2$ , where  $n$  is an integer greater than zero,  $f_c$  is the cutoff frequency of the beam-pipe and  $L$  is roughly the distance between the ion pumps.

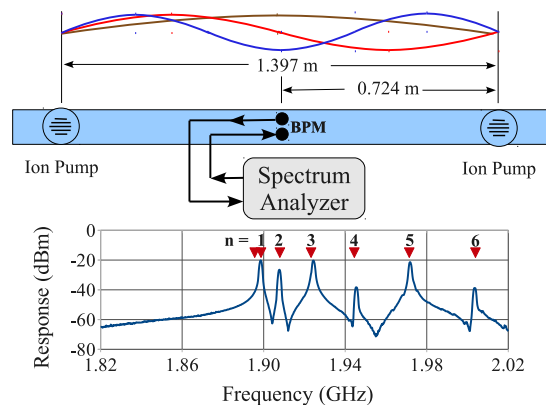


Figure 1: At the location 43E in the CESRTA storage ring, a response measurement shows resonances produced by reflections at two ion pumps. The numbered triangles show the resonant frequencies expected for a rectangular cavity of length  $L = 1.385$  m.

At CESRTA and other accelerators, sections of beam-pipe will often have a resonant response. The analysis to determine

\*Corresponding author. Tel.: +1 6072554882

Email address: jps13@cornell.edu (J.P. Sikora)

the EC density needs to be based on the response of these resonances to changes in EC density [10–12].

## 2. TE Wave Resonance Technique

The natural frequency of a resonator will be shifted by the presence of a plasma within it. In the absence of a magnetic field, the frequency shift is given by Eq. 1, where the integral is taken over the volume of the resonator,  $\nu$  the collision frequency of the plasma and  $\omega_p$  is its plasma frequency [13].

$$\frac{\Delta\omega}{\omega} \approx \left( \frac{1}{1 + (\nu/\omega)^2} \right) \left( \frac{1}{2} \right) \frac{\int_V (\omega_p^2/\omega^2) E_0^2 dV}{\int_V E_0^2 dV} \quad (1)$$

Based on experimental evidence along with theory and simulations, relatively low EC densities are sufficient to produce beam instabilities [2–4]. An EC density of only a few times  $10^{12}$  e-/m<sup>3</sup> is significant, so the collision frequency  $\nu$  will be small and  $\nu/\omega \rightarrow 0$ . There is also a change in the resonator Q at higher plasma densities, but this change is roughly proportional to  $\nu/\omega$ , so changes in Q will not be treated here.

The plasma frequency  $\omega_p$  is related to the plasma (electron cloud) density  $n_e$  by  $n_e = \omega_p^2 \epsilon_0 m_e / e^2$  [14]. Combining this with Eq. 1 for a low density plasma ( $\nu/\omega \rightarrow 0$ ) in the absence of an external magnetic field, the change in resonant frequency for a given EC density  $n_e$  is given by Eq. 2, where the local EC density  $n_e$  can be a function of time and of the position within the resonator.

$$\frac{\Delta\omega}{\omega} \approx \frac{e^2}{2\epsilon_0 m_e \omega^2} \frac{\int_V n_e E_0^2 dV}{\int_V E_0^2 dV} \quad (2)$$

## 3. The Effect of Changes in EC Density on Signals

A fixed frequency drive signal  $\omega$  will produce an equilibrium excitation of a resonator provided that any changes in resonant frequency are slow compared to its damping time. The equilibrium response to a drive signal at a frequency  $\omega$  close to the resonant frequency  $\omega_n$  is given by Eq. 3, where the resonator quality factor Q is related to its damping time  $\tau$  by  $Q = \omega_n \tau / 2$ .

$$x(t) = A_n \sin(\omega t + \phi_n) \quad (3)$$

where

$$A_n = \frac{Q A}{[Q^2(\omega_n^2 - \omega^2)^2 + \omega^4]^{1/2}} \quad (4)$$

$$\phi_n = \tan^{-1} \left[ \frac{Q(\omega_n^2 - \omega^2)}{\omega^2} \right] \quad (5)$$

For a small change in resonant frequency, the change in phase is  $\Delta\phi \approx 2Q\Delta\omega/\omega$ . So with a fixed frequency drive, the equilibrium phase shift due to a change in EC density  $n_e$  is

$$\Delta\phi \approx 2Q \frac{\Delta\omega}{\omega} \approx \frac{Q}{\omega^2} \left( \frac{e^2}{\epsilon_0 m_e} \right) \frac{\int_V n_e E^2 dV}{\int_V E^2 dV}. \quad (6)$$

If  $n_e$  at any given time is assumed to be uniform over this volume, the integrals will simplify and give

$$\Delta\phi \approx \frac{Q}{\omega^2} \frac{e^2}{\epsilon_0 m_e} n_e. \quad (7)$$

If the changes in EC density are *not* slow compared with the resonance damping time, the change in phase is convolved with the  $e^{-t/\tau}$  impulse response of the resonance [15]. For example, if the EC density has a fixed amplitude for a short time interval  $0 \leq t \leq t_0$  and is zero otherwise, the convolved phase shift  $\Delta\Phi$  is given by Eq. 8 and illustrated in the sketch of Fig. 2.

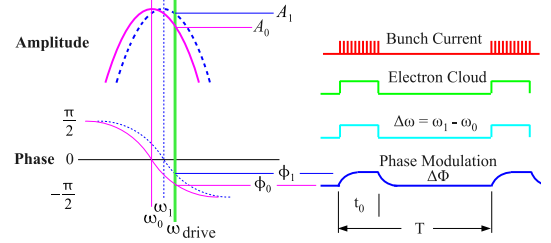


Figure 2: With a fixed drive frequency and a change in resonant frequency rapid compared to the resonance damping time, the phase response will include a convolution as given in Eq. 8. This sketch is for a bunch train of duration  $t_0$  that is short compared to the revolution period  $T$  of the train in a storage ring.

$$\begin{aligned} \Delta\Phi(t) &= \frac{Q}{\omega^2} \frac{e^2}{\epsilon_0 m_e} \int_{-\infty}^t n_e(\xi) e^{-(t-\xi)/\tau} d\xi \quad (8) \\ &= \frac{Q}{\omega^2} \frac{e^2}{\epsilon_0 m_e} n_e (1 - e^{-t/\tau}) \quad 0 \leq t \leq t_0 \\ &= \frac{Q}{\omega^2} \frac{e^2}{\epsilon_0 m_e} n_e (1 - e^{-t_0/\tau}) e^{-(t-t_0)/\tau} \quad t \geq t_0 \end{aligned}$$

At CESRTA, damping times of the beam-pipe resonances are from 400 to 800 ns, while changes in EC density are generally on a shorter time scale. So convolution of the phase shift with the impulse response of the resonance is needed in order to accurately calculate the phase modulation spectra.

## 4. Calculating Spectra

With a periodic beam, such as a short train of bunches in a storage ring, the EC density will vary from a low or zero value to a peak value during one period. This will generate a modulation of the resonant frequency and corresponding amplitude and phase modulation as sketched in Fig. 2. The spectra calculated here are based only on the phase modulation of the signal. As long as the excitation is very close to resonance, the effects of amplitude modulation only become relevant at much higher EC

densities. Frequency modulation can also be an important component of the spectrum, but additional data is needed to confirm this part of the analysis [16, 17].

While it is possible to observe the phase shift by direct phase detection [18], a more sensitive measurement is made by observing the phase modulation sidebands of a fixed drive frequency. A drive signal at frequency  $\omega$  with a small cosine phase modulation of magnitude  $M \ll 1$  and frequency  $\omega_T$ , can be written as in Eq. 9. Using trigonometric identities, the result is a signal at the drive frequency  $\omega$  and sidebands at frequencies  $\omega_T$  above and below the drive frequency, both sidebands having an amplitude  $M/2$  with respect to the drive.

$$\begin{aligned} g(t) &= \sin[\omega t + M \cos(\omega_T t)] \\ &\approx \sin(\omega t) \\ &\quad + \frac{M}{2} [\cos(\omega + \omega_T)t + \cos(\omega - \omega_T)t] \end{aligned} \quad (9)$$

Any periodic phase modulation, such as that described by Eq. 8 of the previous section, can be expressed as a Fourier series  $\Delta\Phi = \sum_{m=1}^{+\infty} C_m \cos(m\omega_T t)$  and each component of that series will produce a pair of sidebands. The phase of each component has been dropped since there is only one component at each sideband frequency and only the magnitude of the sideband is needed to calculate the spectrum.

$$\begin{aligned} g(t) &= \sin[\omega t + \Delta\Phi(t)] \\ &= \sin\left[\omega t + \sum_{m=1}^{+\infty} C_m \cos(m\omega_T t)\right] \\ &\approx \sin(\omega t) \\ &\quad + \sum_{m=1}^{+\infty} \frac{C_m}{2} [\cos(\omega + m\omega_T)t + \cos(\omega - m\omega_T)t] \end{aligned} \quad (10)$$

If the shape of the modulation is known, the Fourier coefficients  $C_m$  of Eq. 10 can be calculated and the sideband amplitudes will be  $C_m/2$  times the amplitude at the drive frequency. With a bunch train in a storage ring with period  $T$ , the revolution frequency of the train is  $\omega_T = 2\pi/T$  and the sidebands are at multiples of this frequency above and below the drive frequency.

## 5. EC Density Measurements

### 5.1. Hardware Setup

Data is taken by coupling microwaves into the beam-pipe, typically using pairs of 18 mm diameter BPM buttons that are driven differentially to couple into the desired mode. Differential drive can be obtained using a  $180^\circ$  splitter/combiner and two equal lengths of cable connected to the buttons. An alternative uses a  $0^\circ$  splitter and two cables of different lengths such that the two buttons are driven with opposite phases at the drive frequency. With elliptical beam-pipe, a TE mode is driven with

a vertically oriented electric field as shown in Fig. 3. In round beam-pipe both horizontal and vertical orientations of the field are possible since they have nearly the same cutoff frequency. All of the data that we have taken so far has used the fundamental mode, with the largest transverse dimension of the beam-pipe being approximately one half wavelength of the excitation frequency.

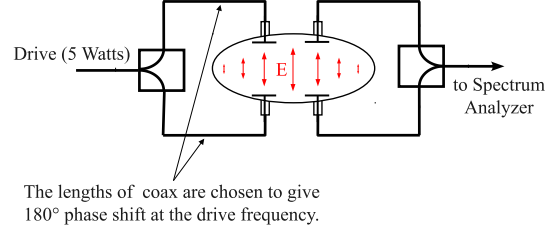


Figure 3: Microwaves excite the beam-pipe in the fundamental waveguide mode using beam position monitor buttons.

As shown in Fig. 4, a drive signal is amplified to the level of roughly 5 W, and passes through a circulator and bandpass filter before being routed to the beam-pipe with low loss cable. The response of the beam-pipe to this drive signal is detected with a second pair of BPM buttons, routed through a 10 dB attenuator and bandpass filter before being recorded with a spectrum analyzer. The bandpass filters and attenuator serve to protect the equipment from the large, wideband direct beam signal. Resonance peaks are found by scanning the drive frequency within 100 MHz of the beam-pipe cutoff frequency and observing the response with a spectrum analyzer – typically without beam in the storage ring. A single drive frequency is chosen that is on or very close to one of the observed resonances.

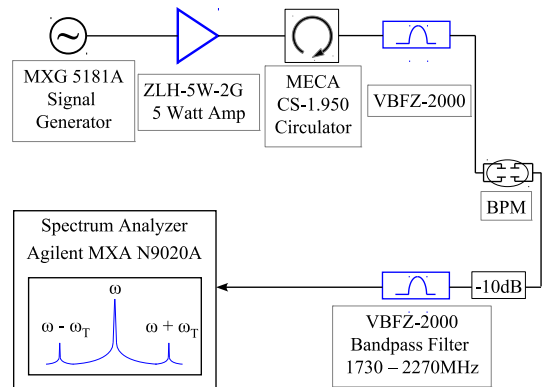


Figure 4: The hardware for TE wave measurements includes a signal generator to excite the beam-pipe and a spectrum analyzer to measure the response.

Figure 5 shows the resonant response at the location 15E at CESRTA in a bare aluminum chamber. As in the example of Fig. 1, resonances are established between two ion pumps where longitudinal slots produce reflections.

### 5.2. Comparing a Measured Spectrum with Calculation

Figure 6 shows the drive and sideband amplitudes measured at 15E with a 10-bunch train of positrons having 14 ns spacing

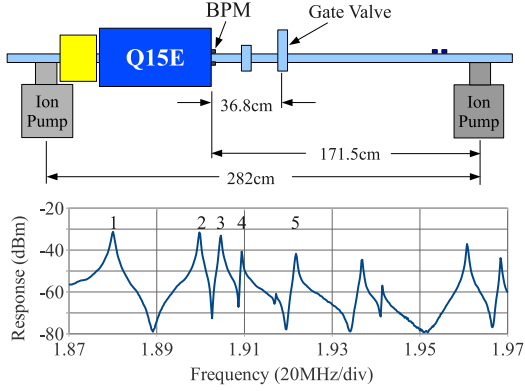


Figure 5: Five resonances at the 15E location of CESRTA are used to measure the EC density in that section of beam-pipe.

(train length 126 ns) and a beam energy of 5.3 GeV. The bunch charge is  $10^{11}$  positrons/bunch (60 mA total current) and the drive frequency is close to the first resonance of Fig. 5, just below 1.88 GHz.

The 10-bunch train is short compare with the 2562 ns revolution period of the storage ring. Using the approximations of the previous section, where the EC density has a fixed value for the 126 ns length of the train and is zero otherwise, the envelope of the sidebands is calculated and shown in Fig. 6. Two envelopes are shown, the first takes into account the beam-pipe response time through the convolution of Eq. 8, using the measured resonance damping time of 500 ns. The second envelope is for a resonance damping time that approaches zero, where the phase shift follows the step changes in EC density instantaneously. Using the relation between the EC density and the spectrum described in the previous section, an EC density of  $4 \times 10^{13}$  e-/m<sup>3</sup> gives a match at the first ( $m = 1$ ) sidebands. For larger values of  $m$ , the sideband envelope that includes convolution with 500 ns remains within about 2 dB of the measured values up to  $m = 10$ .

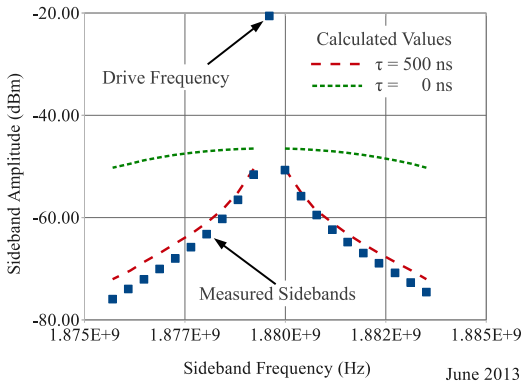


Figure 6: With a 10-bunch train of positrons, measured sidebands are shown as squares with a drive frequency close to the first resonance of Fig. 5. Calculated sideband envelopes from phase modulation are also shown, including convolution with a resonance damping times of 500 ns and 0 ns.

### 5.3. EC Density versus Beam Current

Data has also been taken at 15E where the drive frequency is set to each of the five resonances shown in Fig. 5 where only the first ( $m = 1$ ) upper and lower sidebands are measured. The difference between the amplitude of the received drive (carrier) and the sideband amplitudes in decibels (dBc) is related to the signal magnitudes by  $\text{dBc} = 20 \log(S_m)$  where  $S_m = V_{\text{sideband}}/V_{\text{carrier}}$ . The EC density is calculated from the measured ratio  $S_m$  and the measured  $Q$  of each resonance, assuming that  $n_e$  is uniform over the volume. This is given in Eq. 11, where  $m$  is the sideband index (in this case always equal to one),  $S_m$  is the measured sideband ratio,  $\omega$  the drive frequency and  $C_m$  is the Fourier coefficient of the convolved phase modulation  $\Delta\Phi$  given by Eq. 10.

$$n_e \approx S_m \frac{\omega^2}{Q \cdot C_m} \frac{\epsilon_0 m_e}{e^2} \quad (11)$$

Data was taken with a 10-bunch train of 5. GeV positrons with 14 ns spacing at beam currents up to 80 mA total ( $1.28 \times 10^{11}$  positrons/bunch). The EC density for each resonance calculated to produce the plot in Fig. 7.

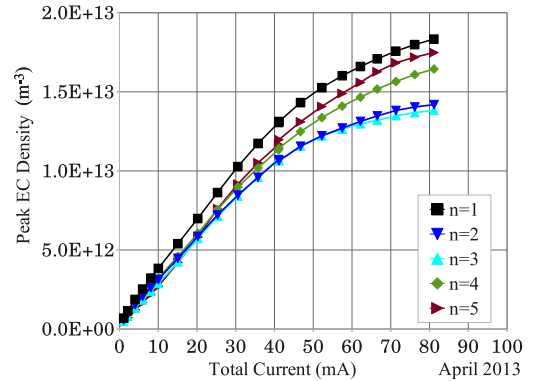


Figure 7: The EC density  $n_e$  is calculated from the ratio  $S_1$  for each of five resonant frequencies and plotted as a function of total beam current in a 10-bunch train of positrons.

### 5.4. Sensitivity of the Measurement

The sensitivity of this technique can be understood through Eq. 11. The value of the drive frequency  $\omega$  and the  $Q$  of the resonance are determined by the beam-pipe geometry. With  $Q$  values of several thousand, the signal level at resonance can be 0 dBm or higher. So the minimum measurable  $n_e$ , which corresponds to the minimum measurable sideband to drive ratio  $S_m$ , is set by the dynamic range of the spectrum analyzer rather than its noise floor. The Agilent MXA 9020 has a dynamic range of 78 dB. Sensitivity to small values of  $n_e$  would also be greatest when the value of  $C_m$  is maximized. This is why the first upper and lower ( $m = 1$ ) sidebands are used in most measurements.  $C_1$  would be further maximized if the ratio of the train length  $t_0$  to the revolution period  $T$  were equal to  $1/2$ , since  $C_1$  is proportional to  $\sin(\pi t_0/T)$ .

At CESR-TA, typical values would be:  $Q = 3000$ ,  $\omega = 2\pi \cdot (2 \text{ GHz})$ , and  $C_1$  (for a 10-bunch train) = 0.06. So with -78 dBc sidebands, the value of  $n_e$  would be  $7 \times 10^{10} \text{ m}^{-3}$ .

## 6. Field Distribution of a Resonance

In the measurements of the previous section, it is assumed that the EC density is uniform over the volume of the resonant beam-pipe, and that the resonance is confined to the region between the two ion pumps. In practice, the EC density will generally not be uniform over the volume, especially when chamber vacuum surfaces are coated with materials intended minimize the production of electron cloud. It is also difficult to infer the field distribution of the resonance except in the simplest cases. When the EC density varies with position in the chamber it is important to know the field distribution of the resonance since from Eq. 6 this determines the contribution of each part of the chamber to the measurement.

### 6.1. Bead Pull Measurement of the L3 Beam-pipe

We had the opportunity to measure the resonant field distribution of an assembly of four chambers before they were installed in the L3 section of the storage ring [19]. The 60 cm long chambers have two different cross sections: one round and the other round with grooves on the upper and lower vacuum surfaces. One of each geometry has a vacuum surface of bare aluminum and the other pair has coatings of TiN.

It was found that in the grooved chambers, the field of the lowest two resonant frequencies is mostly confined to the grooved 60 cm sections. This is due to the slightly lower cutoff frequency of the grooved chambers compared with their smooth wall neighbors. This allows the direct comparison of EC density in the two grooved chambers and the mitigating effects of the TiN coating versus a bare aluminum vacuum surface.

To determine the field distribution in the four chamber assembly, a 0.3 cm<sup>3</sup> nylon bead was guided along the axis of the beam-pipe and changes in the resonant frequency recorded. The frequency shift is proportional to the square of the electric field at the location of the bead [20, 21]. Figure 8 shows the result of one of the bead pull measurements, where the resonant field is confined to the aluminum grooved chamber at two frequencies corresponding to  $n = 1, 2$ . Other measurements gave a similar result for the TiN coated grooved chamber at slightly different frequencies and a different drive/receive location.

### 6.2. EC Density Measurements in the L3 Beam-pipe

Based on the bench measurements of the four chamber assembly, appropriate drive points and frequencies allowed independent measurement of the bare aluminum and the TiN coated grooved chambers. Figure 9 compares the EC density versus total beam current for the these two chambers. The plots in Fig. 9 are not normalized to the amount of synchrotron light in each chamber, but the TiN coating shows a significant reduction in EC density even though it is closer to the source of synchrotron light. The beam was a 10-bunch train of 5.3 GeV positrons with 14 ns spacing.

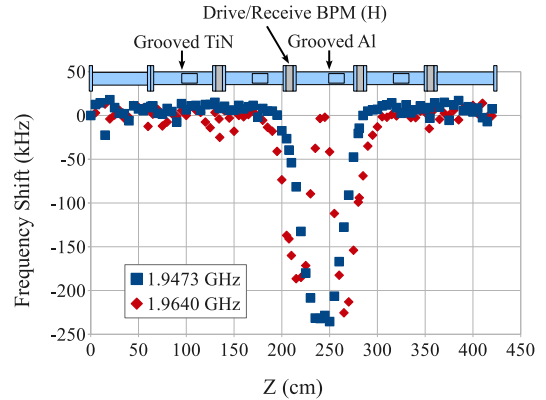


Figure 8: The result of a dielectric bead pull measurement on the four chamber assembly shows two resonances with fields that are primarily within the grooved aluminum chamber.

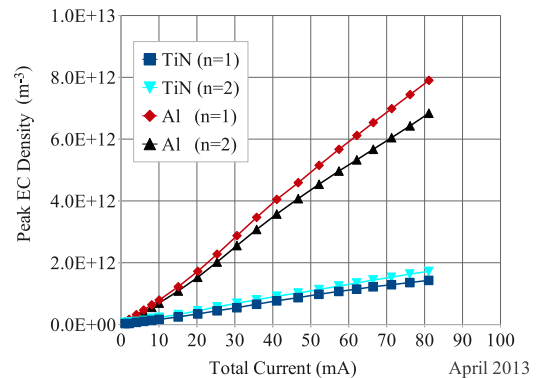


Figure 9: The EC density versus total beam current was measured in the bare aluminum and TiN coated chambers, showing the mitigating effect of the coating. Two resonances were used in each chamber.

## 7. Summary

The EC density in accelerator beam-pipe can be measured by resonantly exciting the beam-pipe with microwaves. Calculations are based on the approximations that the plasma collision frequency  $\nu$  is low, magnetic fields can be neglected and that the sidebands are generated by phase modulation of a fixed drive frequency. When changes in EC density take place on a similar or shorter time scale than the damping time of the resonance, convolution with the resonance impulse response is needed to calculate the phase modulation sidebands. The calculated envelope of the sidebands is in fair agreement with measurements made at CESR-TA of the first ten sidebands. Bead pull measurements are useful in determining the distribution of the resonant field within the beam-pipe. Measurements have shown resonances confined to sections of beam-pipe less than a meter long. A combination of these techniques has been used to show the mitigating effect of a TiN coating on an aluminum chamber.

## 8. Acknowledgements

This work is supported by the US National Science Foundation PHY-0734867, PHY-1002467 and the US Department of

Energy DE-FC02-08ER41538, DE-SC0006505. I am indebted to the work of a number of undergraduate students who were part of the Research Experience for Undergraduates (REU) program of the National Science Foundation. During their relatively brief time here at Cornell, each student made a significant contribution to the development of this technique. They are: Benjamin Carlson (REU 2009): Fourier analysis, frequency shifts due to a plasma, evanescent resonances; Kenneth Hammond (REU 2010): waveguide resonances and simulations; Danielle Duggins (REU 2012): bead pull measurements and waveguide simulations; Alister Tencate (REU 2013) multiple sideband analysis with convolution.

[21] R. G. Carter, "Accuracy of Microwave Cavity Perturbation Measurements," *Microwave Theory and Techniques, IEEE Transactions on*, vol. **49**, no.5, pp.918-923, May 2001

## References

- [1] M.A. Furman and M.T.F. Pivi, "Probabilistic model for the simulation of secondary electron emission," PRST-AB **5**, 124404 (2002).
- [2] M.A. Furman, "Electron Cloud Effects in Accelerators," in Proc. of ELOUD'12, La Biodola, Isola d'Elba, Italy, June 5-8 2012, arXiv:1310.1706 [physics.acc-ph].
- [3] "The CESR-TA: Phase I Report," Tech. Rep. CLNS-12-2084, LEPP, Cornell University, Ithaca, NY (Jan. 2013). <http://www.lns.cornell.edu/public/CLNS/2012/>
- [4] F. Zimmermann, *et al.*, ICFA Beam Dynamics Newsletter No. 33, K. Ohmi & M. Furman, Eds. (2004).
- [5] T. Kroyer, F. Caspers, E. Mahner, "The CERN SPS Experiment on Microwave Transmission Through the Beam Pipe," in Proc of PAC'05, MPPP031, Knoxville, TN, (2004).
- [6] S. De Santis, J. M. Byrd, F. Caspers, *et al*, *Phys. Rev. Lett.* **100**, 094801 (Mar. 2008).
- [7] S. De Santis *et al.*, *Phys. Rev. ST Accel. Beams* **13**, 071002 (Jul. 2010).
- [8] S. Federmann, F. Caspers and E. Mahner, *Phys. Rev. ST Accel. Beams* **14**, 012802 (Jan. 2011).
- [9] G.F. Dugan, *et al.*, ICFA Beam Dynamics Newsletter No. 50, J. Urakawa and W. Chou, Eds. (2009).
- [10] J. P. Sikora, *et al.*, "Resonant TE Wave Measurements of Electron Cloud Densities at CESR-TA," in Proc. of IPAC'11, San Sebastián, Spain, August 2011, TUPC170, p.1434, (2011).
- [11] J. P. Sikora *et al.*, "TE Wave Measurement and Modeling," in Proc. of ELOUD'12, La Biodola, Isola d'Elba, Italy, June 5-8 2012, arXiv:1307.4315 [physics.acc-ph].
- [12] Y.-M. Shin *et al.*, "Microwave Resonator Diagnostics of Electron Cloud Density Profile In High Intensity Proton Beam," in Proc. of IPAC'13, Shanghai, China, May 2013, MOPWA064, pp. 825-827, (2013).
- [13] S. J. Buschbaum & S. C. Brown, *Phys. Rev.* **106**, 196, (1957).
- [14] M. A. Heald and C. B. Wharton, *Plasma Diagnostics with Microwaves*, John Wiley and Sons, New York (1965).
- [15] J.P. Sikora, *et al.*, "Resonant TE Wave Measurement of Electron Cloud Density Using Multiple Sidebands," in Proc. of IBIC'13, Oxford, United Kingdom, September 2013, TUPF34, (2013).
- [16] S. De Santis and J. P. Sikora, *et al.*, "Analysis of Modulation Signals Generated in the TE Wave Detection Method for Electron Cloud Measurements," in Proc. of IPAC'13, New Orleans, United States, May 2012, MOPPR073, (2012).
- [17] S. De Santis and J. P. Sikora, "Analysis of Modulation Signals Generated in the TE Wave Detection Method for Electron Cloud Measurements," in Proc. of IBIC'13, Oxford, United Kingdom, September 2013, TUPF36, (2013).
- [18] J. P. Sikora *et al.*, "Resonant TE Wave Measurements of Electron Cloud Density Using Phase Detection," in Proc. of IBIC'13, Oxford, United Kingdom, September 2013, TUPF35, (2013).
- [19] J. P. Sikora *et al.*, "Electron Cloud Density Measurements Using Resonant TE Waves at CESR-TA," in Proc. of IBIC'12, Tsukuba, Japan, October 2012, TUPB49, (2012).
- [20] L.C. Maier and J.C. Slater, *J. Appl. Phys.* **23**, 68 (1952); doi: 10.1063/1.1701980